
Covariance-aware Feature Alignment with Pre-computed Source Statistics for Test-time Adaptation

Kazuki Adachi¹ Shin’ya Yamaguchi^{1,2} Atsutoshi Kumagai¹

¹NTT Computer and Data Science Laboratories

²Kyoto University

{kazuki.adachi,shinya.yamaguchi,atsutoshi.kumagai}@ntt.com

Abstract

The accuracy of deep neural networks is degraded when the distribution of features in the test environment (target domain) differs from that of the training (source) environment. To mitigate the degradation, test-time adaptation (TTA), where a model adapts to the target domain without access to the source dataset, can be used in the test environment. However, the existing TTA methods lack feature distribution alignment between the source and target domains, which unsupervised domain adaptation mainly addresses, because accessing the source dataset is prohibited in the TTA setting. In this paper, we propose a novel TTA method, named *Covariance-Aware Feature alignment (CAFe)*, which explicitly aligns the source and target feature distributions at test time. To perform alignment without accessing the source data, CAFe uses auxiliary feature statistics (mean and covariance) pre-computed on the source domain, which are lightweight and easily prepared. Further, to improve efficiency and stability, we propose *feature grouping*, which splits the feature dimensions into groups according to their correlations by using spectral clustering to avoid degeneration of the covariance matrix. We empirically show that CAFe outperforms prior TTA methods on a variety of distribution shifts.

1 Introduction

Deep neural networks achieve high accuracy [1, 2, 3] when the training and test datasets can be assumed to have been sampled from the same distribution. However, when this assumption is not satisfied, their performance significantly deteriorates [4, 5, 6]. Unsupervised domain adaptation (UDA) [7] is one of the settings that has been studied actively to address the problem of distribution shift by using labeled data from the training (source) environment (domain) and unlabeled data from the test (target) environment. Most UDA methods focus on minimizing the distribution gap in feature representations between the domains to make the representations invariant to them [8, 9]. Theoretically, since a term for the distribution gap between the domains is included in the expression of the upper bound of the error on the target domain [8, 10, 11], minimizing the gap is a reasonable approach for adapting to the target domain. However, UDA is not always applicable because it requires both a labeled source dataset and an unlabeled target dataset. In fact, access to the source dataset is often restricted due to concerns of privacy, security, copyright, and storage limitation especially after a model has been brought to the target domain [12, 13].

To adapt models to the target domain without accessing the source data, recent studies have addressed a setting called *test-time adaptation (TTA)*, which allows access to only an unlabeled target dataset and a source-pretrained model [14, 15, 16, 17, 18, 19]. This setting is useful for adapting the model after it has been deployed in the target domain. Prior TTA methods mainly focus on adapting batch

normalization (BN) layers or refining output predictions. Methods that adapt BN layers [14, 15, 16, 20] use the dimension-wise statistics (mean and variance) of the BN layers [21] to align the domains. On the other hand, methods that refine the predictions of the models [17, 18, 19] focus on refining the confidence of the predictions on the target domain by using entropy minimization [17, 18], a model ensemble [18], or modifying the weights of the final fully-connected layer [19]. However, their ability to adapt to complex distribution shifts that occur in the real world is limited. In fact, Schneider, et al. [14] report that adapting BN layers works well on uniform distribution shifts such as a single type of image corruption (e.g., noise or blur), but fail to adapt to complex distribution shifts such as mixed types of image corruption. Such situations occur in practice since the environment surrounding the sensors may be unstable and vary with the weather, time, or location, for example. Furthermore, we found that the prior TTA methods other than those that adapt BN layers perform poorly on such complex distribution shifts (see Sec. 5). In summary, these prior works optimize metrics that are hardly related to the source distribution, such as entropy, or incorporate BN statistics that do not sufficiently represent the source distribution. Hence, we hypothesize that the lack of aligned feature distributions limits the performance of TTA. To adapt to distribution shifts more precisely, the target feature distribution should be aligned to the source one like in UDA.

In this paper, we propose a novel TTA method called *Covariance-Aware Feature alignment (CAFe)*. Inspired by UDA [8, 22, 23], CAFe aligns the feature distributions, but does not access the source dataset. To align the distributions precisely, CAFe considers the correlations between the dimensions, instead of just aligning the dimension-wise distributions as is done when adapting BN layers. To do this, we relax the TTA setting to incorporate auxiliary statistics of the source dataset. Concretely, we pre-compute the mean and covariance of the feature representations at training time in the source domain and then fine-tune the model to match the statistics on the target dataset during the TTA step. This does not adversely affect the practicality of TTA, because restoring individual source data from the source statistics is quite difficult. Thus, our method does not violate the privacy concerns. Also, the additional storage space needed for the pre-computed statistics is much smaller than the source model. For example, the source statistics amount to approximately 150KB (it can be further reduced depending on the implementation) in the case of ResNet-50 [3], which is about 100MB in size. Further, if we naively compute the distribution gap with the source statistics, the alignment fails because the target mini-batch covariance matrix degenerates as a result of the batch size being smaller than the number of feature dimensions. To address this issue, we propose *feature grouping* to perform the feature alignment effectively and stably. Feature grouping divides the dimensions of the feature representations into groups on the basis of spectral clustering [24] to find important correlations between the dimensions. We avoid the degeneration problem by aligning the distributions for each group without ignoring important correlations between the dimensions. We empirically show that CAFe outperforms the prior TTA methods on a variety of distribution shifts such as image corruptions and out-of-distribution generalization in Sec. 5.

2 Related Work

Unsupervised domain adaptation (UDA) [7] is an actively studied setting for adapting to distribution shifts. Most UDA methods focus on minimizing the gap in feature distributions between the source and target domains to learn domain-invariant feature representations. For example, DANN [8] and CORAL [22, 23] respectively minimize the \mathcal{H} -divergence and the gap of the covariance matrices of the feature distributions. These approaches are based on the fact that a term for the distribution gap is included in the expression of the upper bound of the generalization error on the target domain [8, 10, 11]. For example, Nguyen, et al. [11] proved the following proposition:

Proposition 1 (Nguyen, et al. [11]) *If the loss $-\log \hat{p}(y|\mathbf{z})$ is bounded by a constant M for $\forall \mathbf{z} \in \mathcal{Z}, y \in \mathcal{Y}$,*

$$l_{test} \leq l_{train} + \frac{M}{2} \sqrt{D_{KL}(p_t(\mathbf{z}) \| p_s(\mathbf{z})) + \mathbb{E}_{p_t(\mathbf{z})}[D_{KL}(p_t(y|\mathbf{z}) \| p_s(y|\mathbf{z}))]}, \quad (1)$$

where \mathbf{z}, y are a feature representation and its label, p_s, p_t are the source and target distributions, $\hat{p}(y|\mathbf{z})$ is the predicted probability, $l_{train} = \mathbb{E}_{p_s(\mathbf{z}, y)}[-\log \hat{p}(y|\mathbf{z})]$, and $l_{test} = \mathbb{E}_{p_t(\mathbf{z}, y)}[-\log \hat{p}(y|\mathbf{z})]$.

Thus, by minimizing the KL-divergence between the two domains, we can expect that the model will make predictions on the target domain as accurately as on the source domain. However, UDA methods cannot be applied to the TTA setting, because UDA requires a labeled source dataset and

unlabeled target dataset at the same time, while TTA allows access to only an unlabeled target dataset. **Source-free domain adaptation** (SFDA) is similar to TTA in terms of adapting to the target domain without accessing the source dataset. SHOT [12] performs pseudo-labeling on the target dataset and then fine-tunes the model with the pseudo-labels. Model adaptation [13] uses a conditional GAN to generate target-style samples and fine-tunes the model on the generated labeled samples. USFDA [25] generates artificial negative samples to learn tighter class boundaries in the training time. The difference between SFDA and TTA is that SFDA is usually done in an offline manner for pseudo-labelling or training additional models. In other words, SFDA requires the whole target dataset to be stored and used for multiple epochs, which is a burden on storage and is computationally expensive. On the other hand, TTA requires no additional models and can adapt in only one epoch, or even in an online manner. This is computationally efficient since each target mini-batch can be discarded once it has been used to update a model and make a prediction (See Appendix C.3). CAFE requires only the pre-computed source statistics and can be used in an online manner.

Test-time adaptation (TTA) fine-tunes the source-pretrained model on the unlabeled target dataset. Unlike SFDA, TTA does not require additional models or running for multiple epochs. Tent [17] minimizes the entropy of the model predictions by optimizing the affine parameters of the BN layers. BACS [18] uses maximum-a-posteriori estimation and a model ensemble in addition to entropy minimization. T3A [19] adjusts the weights of the last fully-connected layer by using the target samples. However, these methods focus on refining the outputs of the model and lack the feature distribution alignment despite that it is important to adapt to the target domain, as mentioned above. In fact, refining the confidence via the entropy of the predictions does not always lead to aligned feature distributions [26]. On the other hand, adapting the BN layers [14, 15, 16, 20] matches the BN statistics to the target ones. This can be regarded as aligning the target feature distribution with the source distribution. However, this method is still incapable of precise feature alignment because the BN layers consider only dimension-wise means and variances, not correlations between dimensions. Moreover, in order to apply this method, a model architecture must include BN layers. More recently, feature restoration (FR) [27], which stores the source feature distribution and aligns the target distribution to it, has been proposed. Here, the problem is that FR cannot capture the feature correlations because FR stores the distribution in the form of a histogram for each feature dimension separately. In contrast to the prior works, inspired by UDA insights of Eq. (1), we decided to focus on aligning the feature distributions more accurately. For the accurate alignment, we seek to match the correlations in addition to the dimension-wise distributions by incorporating pre-computed source statistics. In so doing, we minimize the KL-divergence between the source and target feature distributions and use *feature grouping* for effective and stable feature alignment.

3 Problem Setting

In the TTA setting, a model $f_\theta : \mathcal{X} \mapsto \mathcal{Y}$ is pre-trained on a source dataset $\mathcal{S} = \{(\mathbf{x}_i^s, y_i^s)\} \sim p_s$, where \mathcal{X} and \mathcal{Y} are the input and label space, $\mathbf{x}_i^s \in \mathcal{X}$ and $y_i^s \in \mathcal{Y}$ are a training sample and its label in the source dataset, and p_s is the source distribution over $\mathcal{X} \times \mathcal{Y}$. The goal of TTA is to find the parameter θ^* that can make accurate predictions on the target domain with only an unlabeled target dataset $\mathcal{T} = \{\mathbf{x}_i^t\} \sim p_t$, where $\mathbf{x}_i^t \in \mathcal{X}$ is a target sample and p_t is the target distribution over \mathcal{X} . The label space \mathcal{Y} is shared between the source and target domains. Note that the source dataset \mathcal{S} cannot be accessed during TTA. Instead, we use the statistics (mean and covariance) of the feature representations pre-computed on the source dataset. This does not undermine the advantages of TTA. In fact, source statistics are often used in TTA [14, 15, 16, 20, 27]. For example, the BN layers store the dimension-wise mean and variance of the source domain [21]. Even the parameters of the source-pretrained model themselves can be regarded as a sort of source statistics.

4 Covariance-aware Feature Alignment

Fig. 1 illustrates an overview of CAFE. CAFE is designed to make the target feature distribution close to the source one on the basis of the insights on UDA in Sec. 2. CAFE is divided into two steps:

(Step1) Pre-compute Statistics: First, we compute the statistics (mean and covariance) of the feature representations of the source dataset \mathcal{S} in the training environment with a model f_θ pre-trained on \mathcal{S} (Sec. 4.1). f_θ can be pre-trained with arbitrary training methods or regularization techniques.

(Step2) TTA: We fine-tune f_θ to minimize the *feature alignment loss* on an unlabeled target dataset \mathcal{T} without accessing \mathcal{S} . Using the source statistics computed in the previous step, feature alignment loss

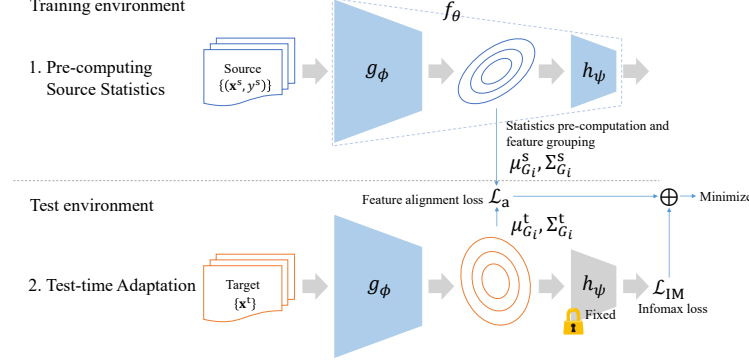


Figure 1: Overview of CAFE.

closes the distribution gap between the source and target domains, and the infomax loss encourages the feature representations to keep clusters that are hard to capture with the feature alignment loss (Sec. 4.2). However, if we compute the feature alignment loss naively, it will diverge because the covariance matrix of the target mini-batch becomes degenerate. Thus, we introduce *feature grouping* to avoid the degenerate matrix and extract important correlations between the dimensions of the feature representations (Sec. 4.3).

4.1 Pre-computing the Statistics

We split the model f_θ into a feature extractor $g_\phi : \mathcal{X} \mapsto \mathbb{R}^d$ and classifier $h_\psi : \mathbb{R}^d \mapsto \mathcal{Y}$, i.e. $f_\theta = h_\psi \circ g_\phi, \theta = [\psi, \phi]$. After training f_θ on the source dataset \mathcal{S} in the training environment, we calculate the mean vector $\mu^s \in \mathbb{R}^d$ and the covariance matrix $\Sigma^s \in \mathbb{R}^{d \times d}$ of the feature representations $\mathbf{z}_i^s = g_\phi(\mathbf{x}_i^s)$ on \mathcal{S} :

$$\mu^s = \frac{1}{|\mathcal{S}|} \sum_{i=1}^{|\mathcal{S}|} \mathbf{z}_i^s, \quad \Sigma^s = \frac{1}{|\mathcal{S}|} \sum_{i=1}^{|\mathcal{S}|} (\mathbf{z}_i^s - \mu^s) (\mathbf{z}_i^s - \mu^s)^\top. \quad (2)$$

4.2 TTA

In this step, we perform TTA in the test environment, where we cannot access the source dataset \mathcal{S} . Here, we present the basic idea of CAFE and then modify it in Sec. 4.3. Instead of \mathcal{S} , we use the source feature statistics μ^s and Σ^s . For each mini-batch of the target dataset \mathcal{T} , we compute the feature statistics μ^t and Σ^t analogously to Eq. (2). Then, we compute the *feature alignment loss* \mathcal{L}_a , which measures the discrepancy of the feature distributions as the KL-divergence of two multivariate Gaussians $\mathcal{N}^t = \mathcal{N}(\mu^t, \Sigma^t)$ and $\mathcal{N}^s = \mathcal{N}(\mu^s, \Sigma^s)$. This can be written in closed form [28]:

$$D_{\text{KL}}(\mathcal{N}^t \parallel \mathcal{N}^s) = \frac{1}{2} \left[\log \frac{\det(\Sigma^s)}{\det(\Sigma^t)} - d + \text{tr} \left(\Sigma^{s-1} \Sigma^t \right) + (\mu^t - \mu^s)^\top \Sigma^{s-1} (\mu^t - \mu^s) \right]. \quad (3)$$

We compute the feature alignment loss \mathcal{L}_a by averaging the KL-divergence in both directions:

$$\mathcal{L}_a = \frac{1}{2} [D_{\text{KL}}(\mathcal{N}^t \parallel \mathcal{N}^s) + D_{\text{KL}}(\mathcal{N}^s \parallel \mathcal{N}^t)]. \quad (4)$$

By minimizing \mathcal{L}_a , the upper bound of the target loss is expected to be tighter since the right-hand side of Eq. (1) has the KL-divergence term between the source and target feature representations. While Eq. (1) has a KL-divergence term for only one direction $D_{\text{KL}}(p_t(\mathbf{z}) \parallel p_s(\mathbf{z}))$, we found that incorporating two directions, which Nguyen et al. [11] recommend, works better.

For measuring the discrepancy of the feature distributions above, we regard them as Gaussians. However, according to the cluster assumption [29], which indicates that natural data form clusters and decision boundaries should lie in low-density regions, the actual feature representations may form clusters such as classes. To keep the clusters, we use the infomax loss [30]:

$$\mathcal{L}_{\text{IM}} = -\frac{1}{B} \sum_{i=1}^B \sum_{j=1}^C \hat{p}_{ij} \log \hat{p}_{ij} + \sum_{j=1}^C \bar{p}_j \log \bar{p}_j, \quad (5)$$

where B is the batch size, C is the number of classes, \hat{p}_{ij} is the softmax probability of the prediction $f_\theta(\mathbf{x}_i^t)$ for the j -th class, and $\bar{p}_j = (1/B) \sum_{i=1}^B \hat{p}_{ij}$. The infomax loss is widely used in (SF)DA [12, 31, 32]. It minimizes the entropy of the individual predictions to encourage data points to keep a certain distance from the decision boundaries, and maximizes the entropy of the averaged probability to encourage the model to make diverse predictions. This helps the features stay clustered.

We fix the classifier h_ψ and optimize the feature extractor g_ϕ to minimize $\mathcal{L}_a + \mathcal{L}_{IM}$.

4.3 Feature Grouping

The basic idea of CAFe is described in Sec. 4.2. However, if we compute Eq. (3) naively, the feature alignment loss \mathcal{L}_a tends to diverge. This is because the target covariance matrix Σ^t calculated over a mini-batch will degenerate and $\det(\Sigma^t)$ become zero since the number of dimensions d (e.g., 2,048 in the case of ResNet-50 [3]) is larger than the ordinary batch size. Hence, before computing \mathcal{L}_a , we perform *feature grouping* to break down the dimensions of the feature representations $\{1, \dots, d\}$ into groups smaller than the batch size and then compute the feature alignment loss for each group.

Since the dimensions of the feature representations are not always independent of each other, we want to split the dimensions into k ($k < d$) groups with strongly-correlated dimensions being put together as much as possible. For this purpose, we use spectral clustering [24], which can split the nodes of a graph into clusters whose nodes are connected to each other. Here, we regard each dimension as a node of a graph and each correlation between the dimensions as a weight of an edge. In other words, we consider a graph with a set of nodes $\mathcal{V} = \{1, \dots, d\}$ and an adjacency matrix $A \in [0, 1]^{d \times d}$ whose elements are the absolute values of the correlation coefficients of the source domain $A_{ij} = |\Sigma_{ij}^s| / \sqrt{\Sigma_{ii}^s \Sigma_{jj}^s}$. We perform spectral clustering on the graph to split the nodes (the dimensions) \mathcal{V} into k clusters (groups). In so doing, the dimensions in the same group will have strong correlations and the dimensions in different groups will have weak correlations. Thus, we consider only intra-group correlations. We denote each group of dimensions by G_1, \dots, G_k . Then, we extract elements corresponding to each group G_i from $\mu^s, \Sigma^s, \mu^t, \Sigma^t$, denoted by $\mu_{G_i}^s \in \mathbb{R}^{|G_i|}, \Sigma_{G_i}^s \in \mathbb{R}^{|G_i| \times |G_i|}, \mu_{G_i}^t \in \mathbb{R}^{|G_i|}, \Sigma_{G_i}^t \in \mathbb{R}^{|G_i| \times |G_i|}$, respectively. The source statistics that we need to bring to the TTA step are only μ^s and $\{\Sigma_{G_i}^s\}_{i=1}^k$ instead of the whole Σ^s . The numbers of parameters of the source statistics are d for μ^s and $\sum_i |G_i|^2$ for $\{\Sigma_{G_i}^s\}_{i=1}^k$. The total number is much smaller than d^2 for Σ^s . The additional storage required in the TTA step is negligible compared to the model size.

Instead of computing the KL-divergence for all dimensions at once as in Eq. (3), we compute it for each group G_i and then average them for \mathcal{L}_a :

$$D_{KL}(\mathcal{N}_{G_i}^t \| \mathcal{N}_{G_i}^s) = \frac{1}{2} \left[\log \frac{\det(\Sigma_{G_i}^s)}{\det(\Sigma_{G_i}^t)} - |G_i| + \text{tr}(\Sigma_{G_i}^{s-1} \Sigma_{G_i}^t) + (\mu_{G_i}^t - \mu_{G_i}^s)^\top \Sigma_{G_i}^{s-1} (\mu_{G_i}^t - \mu_{G_i}^s) \right], \quad (6)$$

$$\mathcal{L}_a = \frac{1}{k} \sum_{i=1}^k \frac{1}{2} [D_{KL}(\mathcal{N}_{G_i}^t \| \mathcal{N}_{G_i}^s) + D_{KL}(\mathcal{N}_{G_i}^s \| \mathcal{N}_{G_i}^t)]. \quad (7)$$

By feature grouping, we can make the number of dimensions for each group $|G_i|$ smaller than the batch size, and thus, $\Sigma_{G_i}^t$ does not degenerate with a proper k (See Sec. 5.8). We assign the uniform weight for each group in Eq. (7) because D_{KL} tends to be larger when $|G_i|$ is large and vice versa, namely, the weights are adaptively changed by the size of G_i .

However, the source covariance $\Sigma_{G_i}^s$ still may degenerate when only a small subspace of the feature space is used on the source domain. To avoid this, we extract the principal components from $\Sigma_{G_i}^s$ and compensate the degenerate directions before computing Eq. (6). Like PCA, the principal components are eigenvectors of $\Sigma_{G_i}^s$, denoted by $V_{G_i} \in \mathbb{R}^{|G_i| \times |G_i|}$, and the variances along the principal components are the corresponding eigenvalues $\lambda_{G_i}^1, \dots, \lambda_{G_i}^{|G_i|}$, s.t. $\Sigma_{G_i}^s V_{G_i} = V_{G_i} \text{diag}(\lambda_{G_i}^1, \dots, \lambda_{G_i}^{|G_i|})$. To improve stability, we clip $\lambda_{G_i}^j$ with a small constant ϵ :

$$\lambda_{G_i}^j \leftarrow \max(\lambda_{G_i}^j, \epsilon). \quad (8)$$

Next, we map the source and target statistics to the space spanned by the source principal components V_{G_i} to measure the KL-divergence with the source statistics modified by Eq. (8):

$$\left(\tilde{\mu}_{G_i}^t, \tilde{\Sigma}_{G_i}^t \right) = \left(V_{G_i} (\mu_{G_i}^t - \mu_{G_i}^s), V_{G_i}^\top \Sigma_{G_i}^t V_{G_i} \right), \quad (9)$$

$$\left(\tilde{\mu}_{G_i}^s, \tilde{\Sigma}_{G_i}^s \right) = \left(V_{G_i} (\mu_{G_i}^s - \mu_{G_i}^s), V_{G_i}^\top \Sigma_{G_i}^s V_{G_i} \right) = \left(\mathbf{0}, \text{diag} \left(\lambda_{G_i}^1, \dots, \lambda_{G_i}^{|G_i|} \right) \right). \quad (10)$$

Finally, we compute the KL-divergence in Eq. (6) with these transformed statistics. The procedure of CAFE is summarized in Appendix D.

5 Experiment

We evaluated CAFE and other TTA methods on various distribution shift benchmarks on image corruption and domain shifts that the previous TTA studies have used. We found that CAFE produces better results for these benchmarks. Further, we found that CAFE especially outperforms the other methods on more complicated distribution shifts with mixed corruption types. We describe the details of the experiment and the datasets in Appendix A and B.

5.1 Dataset

CIFAR: We used CIFAR10/100 [33] as the source datasets and CIFAR10/100-C [4] as the target datasets. CIFAR10/100-C are datasets that are shifted from CIFAR10/100 by applying 15 types of corruption at 5 severity levels to the test set of CIFAR10/100. There are 10,000 images for each corruption type and severity level. We used the images corrupted at the highest severity level. First, we applied TTA to each type of corruption separately as in the previous works [17, 18] (separated sets). Then, we evaluated the TTA methods on a more severely shifted target dataset in which all 15 types of corruption are mixed (mixed set). We randomly sampled 10,000 images from the mixed set to make the dataset the same size as the separated sets.

ImageNet: We used ImageNet [34] as the source dataset and ImageNet-C/R [4, 35] as the target datasets. ImageNet-C is the ImageNet version of CIFAR10/100-C wherein the same types of corruption are applied to the validation set of ImageNet. 50,000 images are included for each corruption type and severity level. Unlike the CIFAR experiment, we used images at all of 5 severity levels. First, we evaluated the TTA methods on each corruption and severity level separately as in the previous studies [17, 18] (separated). Then, we mixed the severity levels and evaluated the TTA methods on each corruption type (severity-mixed) to make the distribution shift harder. Then, we mixed all the corruption types and severity levels (all-mixed). The severity-mixed and all-mixed sets are more realistic distribution shifts because unknown and non-uniform corruptions can occur in the real world. For these sets, we randomly sampled 50,000 images to align the dataset size with the separated sets. We also used ImageNet-R as the target dataset. ImageNet-R consists of 30,000 images of various renditions of 200 ImageNet classes. ImageNet-R has a complicated distribution shift because it includes various renditions such as art, toys, cartoons, etc.

5.2 Pre-training on Source Dataset

We used ResNet-26 [3] in the CIFAR experiments and ResNet-50 in the ImageNet experiments. For the CIFAR experiments, we trained the model on CIFAR10/100 with momentum SGD. We also applied stochastic weight averaging (SWA) [36] and cosine annealing [37]. For the ImageNet experiments, we used the ImageNet-pretrained model provided by Torchvision¹. The detailed settings are described in Appendix A.2.

5.3 Details of CAFE

We used the outputs of the last global-average pooling layer as the feature representations, which have 2,048 dimensions, for both ResNet-26 and ResNet-50. We set the number of groups $k = 128$. For the feature grouping, we used `sklearn.cluster.SpectralClustering` in Scikit-learn [38] with the default hyperparameters. We optimized the feature extractor as described in Sec. 4.2 with momentum SGD for only one epoch, which is a standard setting in TTA. We set `learning_rate` =

¹<https://pytorch.org/vision/stable/index.html>

Table 1: Test accuracy [%] on CIFAR10/100-C. The accuracies on the separated sets are averaged over the corruption types. For each column, the best and second-best accuracies are in **bolded** and underlined.

Method	CIFAR10-C		CIFAR100-C	
	Separated	Mixed	Separated	Mixed
Source	63.75	63.46 ± 0.61	34.24	34.16 ± 0.20
AdaBN [14]	80.26 ± 0.30	67.62 ± 0.13	51.10 ± 0.25	38.52 ± 0.27
T3A [19]	66.02 ± 0.02	63.92 ± 0.42	36.05 ± 0.07	34.10 ± 0.49
Tent [17]	80.86 ± 0.06	68.59 ± 0.30	52.09 ± 0.07	38.95 ± 0.65
BACS [18]	81.51 ± 0.02	68.69 ± 0.09	53.00 ± 0.12	39.65 ± 0.32
FR [27]	80.71 ± 0.40	68.31 ± 0.64	51.50 ± 0.03	39.44 ± 0.32
Infomax [30]	81.40 ± 0.02	69.01 ± 0.50	52.48 ± 0.02	39.78 ± 0.36
CAFe (w/o infomax)	81.11 ± 0.02	69.02 ± 0.62	51.83 ± 0.02	38.71 ± 0.11
CAFe (dimwise)	81.40 ± 0.02	<u>69.10 ± 0.38</u>	52.48 ± 0.02	<u>39.83 ± 0.24</u>
CAFe	81.66 ± 0.01	<u>70.06 ± 0.25</u>	52.79 ± 0.02	<u>40.01 ± 0.36</u>

0.001, and momentum = 0.8. We found that a larger batch size is better and set it to 256 since the target statistics can be estimated precisely. For computational stability, we set $\epsilon = 10^{-5}$ in Eq. (8) (The effect of ϵ is shown in Appendix C.6).

5.4 Baselines

We compare CAFe with these previous TTA methods and variants of CAFe. The detailed settings are given in Appendix A.3.

Source evaluated the source-pretrained model on the target dataset without any adaptation. **Ad-aBN** [14] replaced the statistics of BN layers with the target ones by keeping updating the BN layers during the test run. **Tent** [17] minimized the entropy of the predictions by optimizing the affine parameters γ, β of BN layers. **BACS** [18] minimized the entropy of the predictions by using regularization with the posterior distribution of the parameters. Here, while the original BACS had an ensemble of 10 models for the uncertainty estimation, we used only one model for a fair comparison and practicality. **T3A** [19] updated the weights of the last fully-connected layer by regarding the weights as the prototypes of each class and replacing the prototypes with the mean of the target samples. **FR** [27] minimized the dimension-wise KL-divergence of the feature distributions and the logits between the source and target statistics. Unlike CAFe, the statistics were represented in the form of a histogram. **Infomax** [30] minimized only the infomax loss \mathcal{L}_{IM} for ablation. **CAFe (w/o infomax)** minimized only the feature alignment loss \mathcal{L}_a for ablation. **CAFe (dimwise)** computed the feature alignment loss \mathcal{L}_a ignoring the correlations between the feature dimensions. This is a special case of CAFe ($k = d$), i.e. $G_i = \{i\}$. **DANN** [8] is a representative method of UDA. The results are shown in Appendix C.7.

As in the previous TTA studies [14, 17, 18], we ran each TTA method on the unlabeled target dataset for one epoch and then evaluated the accuracy on the same target dataset. We ran each TTA three times with different random seeds and report the mean and standard deviations. We also evaluated TTA in a batched online manner, where each mini-batch was accessed only one time (see Appendix C.3).

5.5 Results on CIFAR

Tab. 1 shows the test accuracy on CIFAR10/100-C. CAFe outperformed the baselines. Even when the correlations between the features were ignored in \mathcal{L}_a , CAFe (dimwise) still produced competitive results. CAFe had higher accuracy especially on the mixed target dataset. This indicates that aligning the distributions including covariance enables the models to adapt to more complex distribution shifts. On the other hand, CAFe (w/o infomax) had poorer accuracy compared with the other CAFe variants. This suggests that regarding the feature distributions as multivariate Gaussians in \mathcal{L}_a hardly captures clusters of features and that the infomax loss works complementarily.

Table 2: Test accuracy [%] on ImageNet-C/R. The accuracies on the separated sets are averaged over the corruption types and severity levels. The accuracies on the severity-mixed sets are averaged over the corruption types. The best and second-best accuracies in each column are in **bolded** and underlined.

Method	Separated	ImageNet-C		ImageNet-R
		Severity-mixed	All-mixed	
Source	39.14	39.43 ± 0.00	39.16 ± 0.01	36.17
AdaBN [14]	50.28 ± 0.02	48.00 ± 0.17	39.85 ± 0.18	39.91 ± 0.29
T3A [19]	39.05 ± 0.01	39.28 ± 0.03	37.46 ± 0.09	35.09 ± 0.12
Tent [17]	58.97 ± 0.03	57.15 ± 0.05	44.44 ± 0.22	43.35 ± 0.17
BACS [18]	57.01 ± 0.19	55.05 ± 0.29	33.07 ± 1.38	39.29 ± 0.78
FR [27]	53.54 ± 0.01	50.38 ± 0.20	40.52 ± 0.16	40.39 ± 0.02
Infomax [30]	60.20 ± 0.05	57.52 ± 0.23	46.52 ± 0.08	46.05 ± 0.03
CAFe (w/o infomax)	57.35 ± 0.02	54.43 ± 0.14	43.83 ± 0.16	39.54 ± 0.10
CAFe (dimwise)	<u>60.29 ± 0.08</u>	<u>58.60 ± 0.36</u>	<u>47.19 ± 0.24</u>	<u>45.88 ± 0.08</u>
CAFe	60.77 ± 0.09	59.04 ± 0.22	48.55 ± 0.26	44.94 ± 0.19

Table 3: Fréchet distances of the feature representations between the source and target datasets after TTA. The target dataset is ‘mixed’ for CIFAR10/100-C and ‘all-mixed’ for ImageNet-C.

Method	CIFAR10-C	CIFAR100-C	ImageNet-C	ImageNet-R
Source	1.39	17.36	68.24	96.25
Tent [17]	0.15	5.96	26.75	37.09
BACS [18]	0.14	6.70	101.53	60.11
FR [27]	7629	5.85	27.86	35.08
CAFe (w/o infomax)	0.080	5.37	17.13	26.72
CAFe (dimwise)	0.075	5.77	32.95	51.91
CAFe	0.026	5.35	20.27	35.63

5.6 Results on ImageNet

Tab. 2 shows the test accuracy on ImageNet-C/R. For ImageNet-C, CAFe outperformed the baselines in all cases. Especially in the all-mixed case, CAFe had significantly higher accuracy. This implies that aligning the feature distributions becomes more important when the distribution shift is complicated. On the other hand, in ImageNet-R, although CAFe was competitive, Infomax outperformed the best. This is because of the change in the label space. ImageNet-R has only 200 subclasses of the 1,000 classes of ImageNet. Thus, aligning the source and target feature distributions harmed the target feature distribution. We additionally calculated the source feature statistics on the 200 subclasses of ImageNet and ran CAFe on ImageNet-R with the statistics. This resulted in $45.84 \pm 0.16\%$ of test accuracy, a slight improvement compared to CAFe using the source statistics over the 1,000 classes. The details are shown in Tab. 1 and Tab. 2 in Appendix C.1.

5.7 Effect of the Feature Alignment

We measured how close the distribution distance between the source and target datasets became as a result of using the feature alignment loss. After TTA, we calculated the mean μ^t and covariance Σ^t for each target dataset and evaluated the Fréchet distance between the two domains (see Appendix A.4). Tab. 3 shows that CAFe effectively closed the distribution gap. By considering the covariance, CAFe reduced the gap more than CAFe (dimwise) did. On the other hand, for ImageNet-C/R, CAFe (w/o infomax) reduced the gap the most since its objective is only the feature alignment loss. However, its accuracy was not the best because the infomax loss is necessary for keeping the clusters.

5.8 Effect of the Feature Grouping

We examined the effect of the number of groups k in the feature grouping. Tab. 4 shows the test accuracy of CAFe on CIFAR100-C (Mixed) and ImageNet-C (All-mixed) for each group size k . k affects the number of correlations between the feature dimensions to be considered. Using smaller k , more correlations are considered because the size of each group G_i increases. In the case of

Table 4: Test accuracy of CAFE on CIFAR100-C (Mixed) and ImageNet-C (All-mixed) for each group size k . The best accuracy on each datasets is **bolded**. N/A means that CAFE did not work.

k	CIFAR100-C (Mixed)	ImageNet-C (All-mixed)
8	N/A	N/A
16	N/A	0.11 ± 0.02
32	41.06 ± 0.18	46.22 ± 0.16
64	40.67 ± 0.21	48.58 ± 0.13
128	40.01 ± 0.36	48.55 ± 0.26
256	39.60 ± 0.10	48.21 ± 0.31
512	N/A	N/A
1024	39.70 ± 0.09	N/A

CIFAR100-C (Mixed), $k = 32$ gives in the best accuracy. This is because the distributions are aligned accurately. However, when $k \leq 16$, CAFE does not work because some of the feature groups are larger than the batch size. For G_i larger than the batch size, the KL-divergence in Eq. (6) diverges since $\det(\Sigma_{G_i}^t) = 0$ for a mini-batch. For ImageNet-C (All-mixed), $k = 64$ gives the best accuracy. In the $k \leq 32$ cases, the accuracies decrease. This is because the covariance estimation becomes inaccurate as the number of dimensions of the feature groups increases. On the other hand, in some cases of larger k , the spectral clustering produces a few large feature groups and many small ones. Thus, the KL-divergences for the large groups diverge. We can also see that the choice of k does not largely affect accuracy in most cases when CAFE works. Practically speaking, we recommend choosing k such that the feature group size is sufficiently smaller than the batch size B , i.e. $k > d/B$. The relationship between the size of the feature groups and k is visualized in Appendix C.2.

6 Conclusion

We proposed a novel TTA method, called Covariance-Aware Feature alignment (CAFE), which aligns the target feature distribution to the source distribution. We also proposed feature grouping, to extract important correlations between the feature dimensions by spectral clustering and improve computing stability. CAFE effectively closes the distribution gap and improves test accuracy on various distribution shifts without having to access the source dataset. One of the limitations of CAFE is the conditional distribution alignment. Since CAFE aligns the marginal distribution $p(\mathbf{z})$ of the two domains, the conditional distributions $p(\mathbf{z}|y)$ are not always aligned. One of the directions of future work would be to deal with this conditional distribution alignment, UDA addressed this issue recently [39, 40]. Another potential drawback is that tracking the behavior of the adapted models can be difficult. This may have ethical concerns such as fairness in some sensitive applications. We hope that the TTA setting can be extended to various distribution shifts as well as UDA.

References

- [1] Alex Krizhevsky, Ilya Sutskever, and Geoffrey E Hinton. Imagenet classification with deep convolutional neural networks. In *Advances in neural information processing systems*, pages 1097–1105, 2012.
- [2] K. Simonyan and Andrew Zisserman. Very Deep Convolutional Networks for Large-Scale Image Recognition. *CoRR*, abs/1409.1556, 2015.
- [3] Kaiming He, Xiangyu Zhang, Shaoqing Ren, and Jian Sun. Deep residual learning for image recognition. In *Proceedings of the IEEE conference on computer vision and pattern recognition (CVPR)*, pages 770–778, 2016.
- [4] Dan Hendrycks and Thomas Dietterich. Benchmarking Neural Network Robustness to Common Corruptions and Perturbations. *Proceedings of the International Conference on Learning Representations (ICLR)*, 2019.
- [5] Benjamin Recht, Rebecca Roelofs, Ludwig Schmidt, and Vaishaal Shankar. Do imagenet classifiers generalize to imagenet? In *International Conference on Machine Learning*, pages 5389–5400. PMLR, 2019.

- [6] Robert Geirhos, Carlos R. M. Temme, Jonas Rauber, Heiko H. Schütt, Matthias Bethge, and Felix A. Wichmann. Generalisation in humans and deep neural networks. In S. Bengio, H. Wallach, H. Larochelle, K. Grauman, N. Cesa-Bianchi, and R. Garnett, editors, *Advances in Neural Information Processing Systems*, volume 31. Curran Associates, Inc., 2018.
- [7] Gabriela Csurka. Domain adaptation for visual applications: A comprehensive survey. *arXiv preprint arXiv:1702.05374*, 2017.
- [8] Yaroslav Ganin, Evgeniya Ustinova, Hana Ajakan, Pascal Germain, Hugo Larochelle, François Laviolette, Mario Marchand, and Victor Lempitsky. Domain-adversarial training of neural networks. *The Journal of Machine Learning Research*, 17(1):2096–2030, 2016.
- [9] Mingsheng Long, ZHANGJIE CAO, Jianmin Wang, and Michael I Jordan. Conditional Adversarial Domain Adaptation. In S. Bengio, H. Wallach, H. Larochelle, K. Grauman, N. Cesa-Bianchi, and R. Garnett, editors, *Advances in Neural Information Processing Systems*, volume 31. Curran Associates, Inc., 2018.
- [10] Shai Ben-David, John Blitzer, Koby Crammer, Alex Kulesza, Fernando Pereira, and Jennifer Wortman Vaughan. A theory of learning from different domains. *Machine learning*, 79(1):151–175, 2010.
- [11] A Tuan Nguyen, Toan Tran, Yarin Gal, Philip HS Torr, and Atilim Güneş Baydin. KL Guided Domain Adaptation. *International Conference on Learning Representations*, 2022.
- [12] Jian Liang, Dapeng Hu, and Jiashi Feng. Do we really need to access the source data? source hypothesis transfer for unsupervised domain adaptation. In *International Conference on Machine Learning (ICML)*, pages 6028–6039. PMLR, 2020.
- [13] Rui Li, Qianfen Jiao, Wenming Cao, Hau-San Wong, and Si Wu. Model Adaptation: Unsupervised Domain Adaptation Without Source Data. In *Proceedings of the IEEE/CVF Conference on Computer Vision and Pattern Recognition (CVPR)*, June 2020.
- [14] Steffen Schneider, Evgenia Rusak, Luisa Eck, Oliver Bringmann, Wieland Brendel, and Matthias Bethge. Improving robustness against common corruptions by covariate shift adaptation. *Advances in Neural Information Processing Systems*, 33, 2020.
- [15] Yanghao Li, Naiyan Wang, Jianping Shi, Jiaying Liu, and Xiaodi Hou. Revisiting Batch Normalization For Practical Domain Adaptation. In *International Conference on Learning Representations Workshop*, 2017.
- [16] Philipp Benz, Chaoning Zhang, Adil Karjauv, and In So Kweon. Revisiting Batch Normalization for Improving Corruption Robustness. In *Proceedings of the IEEE/CVF Winter Conference on Applications of Computer Vision (WACV)*, pages 494–503, January 2021.
- [17] Dequan Wang, Evan Shelhamer, Shaoteng Liu, Bruno Olshausen, and Trevor Darrell. Tent: Fully Test-Time Adaptation by Entropy Minimization. *International Conference on Learning Representations (ICLR)*, 2021.
- [18] Aurick Zhou and Sergey Levine. Bayesian Adaptation for Covariate Shift. *Advances in Neural Information Processing Systems*, 34, 2021.
- [19] Yusuke Iwasawa and Yutaka Matsuo. Test-time classifier adjustment module for model-agnostic domain generalization. *Advances in Neural Information Processing Systems*, 34, 2021.
- [20] Masato Ishii and Masashi Sugiyama. Source-free Domain Adaptation via Distributional Alignment by Matching Batch Normalization Statistics. *arXiv preprint arXiv:2101.10842*, 2021.
- [21] Sergey Ioffe and Christian Szegedy. Batch Normalization: Accelerating Deep Network Training by Reducing Internal Covariate Shift. In Francis Bach and David Blei, editors, *Proceedings of the 32nd International Conference on Machine Learning (ICML)*, volume 37 of *Proceedings of Machine Learning Research*, pages 448–456, Lille, France, 07–09 Jul 2015. PMLR.
- [22] Baochen Sun and Kate Saenko. Deep coral: Correlation alignment for deep domain adaptation. In *European conference on computer vision*, pages 443–450. Springer, 2016.

[23] Baochen Sun, Jiashi Feng, and Kate Saenko. Return of frustratingly easy domain adaptation. In *Proceedings of the AAAI Conference on Artificial Intelligence*, volume 30, 2016.

[24] Charles J Alpert and So-Zen Yao. Spectral partitioning: The more eigenvectors, the better. In *Proceedings of the 32nd annual ACM/IEEE design automation conference*, pages 195–200, 1995.

[25] Jogendra Nath Kundu, Naveen Venkat, R Venkatesh Babu, et al. Universal source-free domain adaptation. In *Proceedings of the IEEE/CVF Conference on Computer Vision and Pattern Recognition (CVPR)*, pages 4544–4553, 2020.

[26] Pietro Morerio, Jacopo Cavazza, and Vittorio Murino. Minimal-Entropy Correlation Alignment for Unsupervised Deep Domain Adaptation. In *International Conference on Learning Representations*, 2018.

[27] Cian Eastwood, Ian Mason, Chris Williams, and Bernhard Schölkopf. Source-Free Adaptation to Measurement Shift via Bottom-Up Feature Restoration. In *International Conference on Learning Representations*, 2022.

[28] John Duchi. Derivations for Linear Algebra and Optimization, 2007. http://ai.stanford.edu/~jduchi/projects/general_notes.pdf.

[29] Olivier Chapelle and Alexander Zien. Semi-supervised classification by low density separation. In *International workshop on artificial intelligence and statistics*, pages 57–64. PMLR, 2005.

[30] John Bridle, Anthony Heading, and David MacKay. Unsupervised Classifiers, Mutual Information and 'Phantom Targets. In J. Moody, S. Hanson, and R. P. Lippmann, editors, *Advances in Neural Information Processing Systems*, volume 4. Morgan-Kaufmann, 1992.

[31] Tuan-Hung Vu, Himalaya Jain, Maxime Bucher, Matthieu Cord, and Patrick Pérez. Advent: Adversarial entropy minimization for domain adaptation in semantic segmentation. In *Proceedings of the IEEE/CVF Conference on Computer Vision and Pattern Recognition*, pages 2517–2526, 2019.

[32] Kuniaki Saito, Donghyun Kim, Stan Sclaroff, Trevor Darrell, and Kate Saenko. Semi-supervised domain adaptation via minimax entropy. In *Proceedings of the IEEE/CVF International Conference on Computer Vision*, pages 8050–8058, 2019.

[33] Alex Krizhevsky, Geoffrey Hinton, et al. Learning multiple layers of features from tiny images. 2009.

[34] Olga Russakovsky, Jia Deng, Hao Su, Jonathan Krause, Sanjeev Satheesh, Sean Ma, Zhiheng Huang, Andrej Karpathy, Aditya Khosla, Michael Bernstein, Alexander C. Berg, and Li Fei-Fei. ImageNet Large Scale Visual Recognition Challenge. *International Journal of Computer Vision (IJCV)*, 115(3):211–252, 2015.

[35] Dan Hendrycks, Steven Basart, Norman Mu, Saurav Kadavath, Frank Wang, Evan Dorundo, Rahul Desai, Tyler Zhu, Samyak Parajuli, Mike Guo, Dawn Song, Jacob Steinhardt, and Justin Gilmer. The Many Faces of Robustness: A Critical Analysis of Out-of-Distribution Generalization. *arXiv preprint arXiv:2006.16241*, 2020.

[36] Wesley J Maddox, Pavel Izmailov, Timur Garipov, Dmitry P Vetrov, and Andrew Gordon Wilson. A simple baseline for bayesian uncertainty in deep learning. *Advances in Neural Information Processing Systems*, 32:13153–13164, 2019.

[37] Frank Hutter Ilya Loshchilov. SGDR: stochastic gradient descent with warm restarts. In *International Conference on Learning Representations (ICLR)*, 2017.

[38] Fabian Pedregosa, Gaël Varoquaux, Alexandre Gramfort, Vincent Michel, Bertrand Thirion, Olivier Grisel, Mathieu Blondel, Peter Prettenhofer, Ron Weiss, Vincent Dubourg, Jake Vanderplas, Alexandre Passos, David Cournapeau, Matthieu Brucher, Matthieu Perrot, and Édouard Duchesnay. Scikit-learn: Machine Learning in Python. *Journal of Machine Learning Research*, 12(85):2825–2830, 2011.

- [39] Han Zhao, Remi Tachet Des Combes, Kun Zhang, and Geoffrey Gordon. On learning invariant representations for domain adaptation. In *International Conference on Machine Learning*, pages 7523–7532. PMLR, 2019.
- [40] Trung Le, Tuan Nguyen, Nhat Ho, Hung Bui, and Dinh Phung. LAMDA: Label Matching Deep Domain Adaptation. In Marina Meila and Tong Zhang, editors, *Proceedings of the 38th International Conference on Machine Learning*, volume 139 of *Proceedings of Machine Learning Research*, pages 6043–6054. PMLR, 18–24 Jul 2021.
- [41] Adam Paszke, Sam Gross, Francisco Massa, Adam Lerer, James Bradbury, Gregory Chanan, Trevor Killeen, Zeming Lin, Natalia Gimelshein, Luca Antiga, Alban Desmaison, Andreas Kopf, Edward Yang, Zachary DeVito, Martin Raison, Alykhan Tejani, Sasank Chilamkurthy, Benoit Steiner, Lu Fang, Junjie Bai, and Soumith Chintala. PyTorch: An Imperative Style, High-Performance Deep Learning Library. In H. Wallach, H. Larochelle, A. Beygelzimer, F. d’Alché-Buc, E. Fox, and R. Garnett, editors, *Advances in Neural Information Processing Systems 32*, pages 8024–8035. Curran Associates, Inc., 2019.
- [42] V. Fomin, J. Anmol, S. Desroziers, J. Kriss, and A. Tejani. High-level library to help with training neural networks in pytorch. <https://github.com/pytorch/ignite>, 2020.
- [43] Ross Wightman. Pytorch image models. <https://github.com/rwightman/pytorch-image-models>, 2019.
- [44] D.C Dowson and B.V Landau. The Fréchet distance between multivariate normal distributions. *Journal of Multivariate Analysis*, 12(3):450–455, 1982.
- [45] Yuval Netzer, Tao Wang, Adam Coates, Alessandro Bissacco, Bo Wu, and Andrew Y Ng. Reading digits in natural images with unsupervised feature learning. 2011.
- [46] Yann LeCun, Corinna Cortes, and Christopher J.C. Burges. MNIST handwritten digit database, 1998. <http://yann.lecun.com/exdb/mnist/>.

A Implementation Details

The implementation used PyTorch [41] and PyTorch-Ignite [42].

A.1 Computing Resources

For training and TTA, we used NVIDIA A100 GPUs of our internal computer cluster. Training the source models and collecting SWAG posterior for CIFAR and ImageNet datasets took approximately 70 hours in total with single GPU. Each TTA took approximately 15 minutes for ImageNet experiments and 1 minutes for CIFAR experiments with single GPU. In total, it took approximately 700 GPU hours to carry out all of TTA experiments in this paper.

A.2 Source Pre-training

ResNet-26 and ResNet-50 that we used are included in timm [43] and Torchvision² libraries.

For CIFAR experiments, we trained ResNet-26 with momentum SGD from scratch. We set `batch_size = 128`, `initial_learning_rate = 0.1`, `momentum = 0.9`, and `weight_decay = 5 × 10-4`. We decayed the learning rate to 0 with cosine annealing [37] over the first 200 epochs. Then, from epoch 200, we fixed `learning_rate = 0.01` and collected SWAG [36] for 100 epochs. For SWAG, the parameters are collected 4 times per epoch. We used the means of the collected parameters as the source model.

For ImageNet experiments, we downloaded the ImageNet-pretrained ResNet-50 via Torchvision (`torchvision.models.resnet50`) by specifying `pretrained=True`. For BACS [18], we further trained the ImageNet-pretrained model on ImageNet to collect the SWAG posterior. We ran vanilla SGD for optimization with `learning_rate = 0.0001` and `batch_size = 128` for 10 epochs and collected the parameters 4 times per epoch.

²<https://pytorch.org/vision/stable/index.html>

A.3 Adaptation

We describe the details of CAFE and other TTA methods. For each condition, we ran adaptation three times with different random seeds and averaged the accuracies.

AdabN [14]: We ran the test run with keeping updating the BN statistics. We set batch size to 32.

BACS [18]: We set the hyperparameters same as [18]. We used momentum SGD for optimization. For CIFAR experiments, we set batch_size = 128, learning_rate = 0.001, momentum = 0.8, and the weight of the posterior term to 0.0001. For ImageNet experiments, we set batch_size = 64, learning_rate = 0.0001, momentum = 0.9, and the weight of the posterior term to 0.0003.

Tent [17]: We set the hyperparameters as [17]. We used momentum SGD for optimization. For CIFAR experiments, we set batch_size = 128, learning_rate = 0.001, and momentum = 0.8. For ImageNet experiments, we set batch_size = 64, learning_rate = 0.00025, and momentum = 0.8.

T3A [19]: We set batch_size = 32 as [19]. For the number of feature vectors to pool M , we searched from $\{1, 5, 20, 50, 100, \infty\}$ and adopted $M = 20$ that consistently performs the best for all experiments.

FR [27]: We omit the bottom up FR since it cannot be applied to TTA. As [27], we set the number of bins to 8, and the temperature parameter of the soft binning to 0.01 for offline and 0.05 for online setting. For optimization, we used momentum SGD and set the learning rate to 0.001 and the momentum to 0.9, and batch size to 256.

CAFe: The hyperparameters are described in Sec. 5.3. For computing the KL-divergence in Eq. (6), we made some modifications for stability. The term $\log \det(\Sigma_{G_i}^s) / \det(\Sigma_{G_i}^t) = \log \det(\Sigma_{G_i}^s) - \log \det(\Sigma_{G_i}^t)$ diverges if we compute it naively because the determinant of the covariance matrices often become near-zero. Thus, we computed it with Cholesky decomposition:

$$\log \det(\Sigma_{G_i}^t) = 2 \sum_{j=1}^{|G_i|} \log L_{jj}, \quad (11)$$

where L is a lower triangular matrix obtained by Cholesky decomposition such that $LL^\top = \Sigma_{G_i}^t$. $\log \det(\Sigma_{G_i}^s)$ is computed as the following since $\Sigma_{G_i}^s$ becomes a diagonal matrix after the transformation in Eq. (10):

$$\log \det(\Sigma_{G_i}^s) = \sum_{j=1}^{|G_i|} \log \lambda_{G_i}^j. \quad (12)$$

A.4 Fréchet Distance

In Sec. 5.7, we measured the distance between the source and target distributions by using the Fréchet distance between the two Gaussians $\mathcal{N}(\mu^t, \Sigma^t)$ and $\mathcal{N}(\mu^s, \Sigma^s)$, which is calculated as [44]:

$$\|\mu^t - \mu^s\|_2^2 + \text{tr} \left(\Sigma^t + \Sigma^s - 2(\Sigma^t \Sigma^s)^{1/2} \right). \quad (13)$$

B Dataset Details

CIFAR10/100 [33]: We downloaded CIFAR10/100 via Torchvision. We could not find the license information for CIFAR10/100.

ImageNet [34]: We downloaded ImageNet from the official site³. ImageNet is released under license that allows it to be used for non-commercial research/educational purposes (see <https://image-net.org/download.php>).

CIFAR10/100-C and ImageNet-C [4]: We downloaded CIFAR10/100-C and ImageNet-C from <https://zenodo.org/record/2535967>, <https://zenodo.org/record/3555552>, and <https://zenodo.org/record/2235448>, which are released by the authors. They are released under the CC BY 4.0 License.

ImageNet-R [35]: We downloaded ImageNet-R from their GitHub repository⁴. It is released under the MIT License.

³<https://www.image-net.org/>

⁴<https://github.com/hendrycks/imagenet-r>

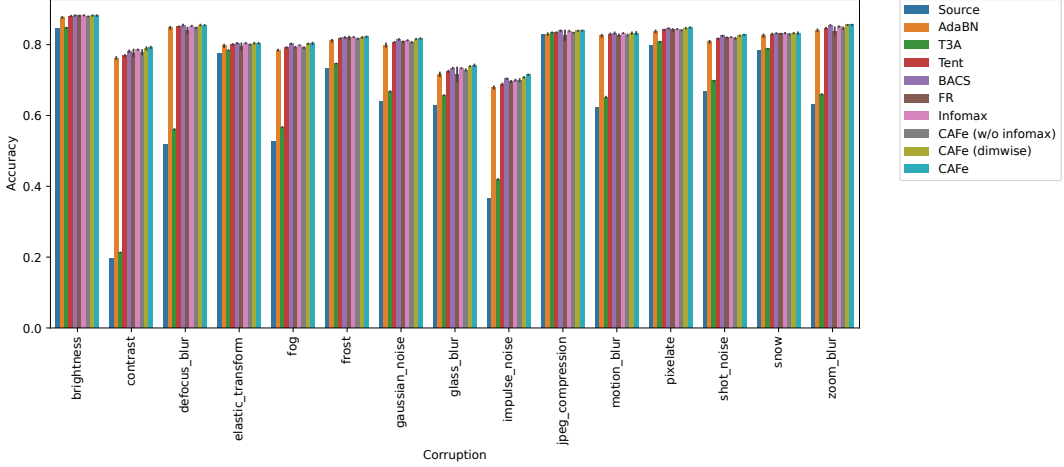


Figure 2: Test accuracy for each corruption type on the separated sets of CIFAR10-C.

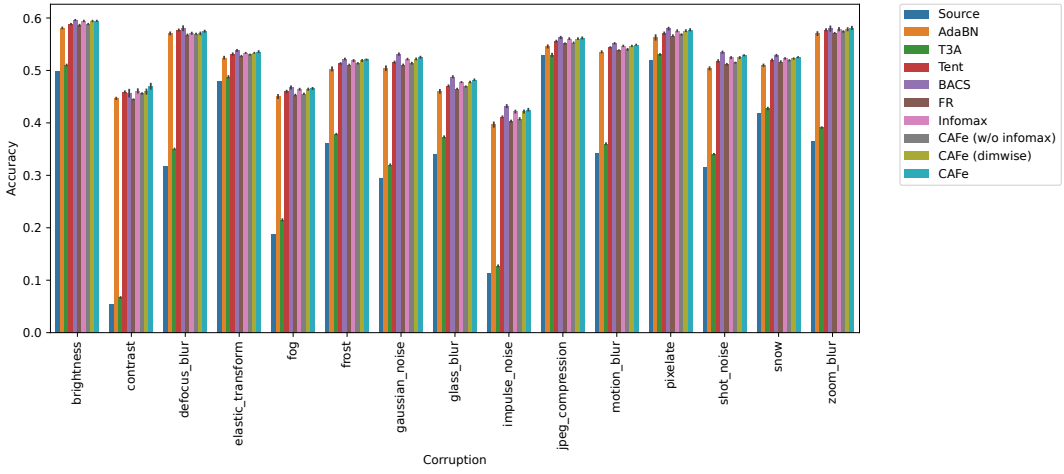


Figure 3: Test accuracy for each corruption type on the separated sets of CIFAR100-C.

SVHN [45]: We downloaded SVHN via Torchvision. It can be used for non-commercial purposes only (see <http://ufldl.stanford.edu/housenumbers/>).

MNIST [46]: We downloaded MNIST via Torchvision. We could not find the license information for MNIST.

C Other Experimental Results

C.1 TTA Result

Fig. 2 – Fig. 5 show the detailed test accuracies on CIFAR-10/100-C and ImageNet-C reported in Tab. 1 and Tab. 2 for each corruption type.

C.2 Feature Grouping

We inspected the size of each groups made by feature grouping. Fig. 6 shows the size of each group for each k on CIFAR100 and ImageNet. When $k \in \{8, 16, 512\}$ on CIFAR100 and $k \in \{8, 512, 1024\}$ on ImageNet, groups that are larger than the batch size occur. In these cases, the

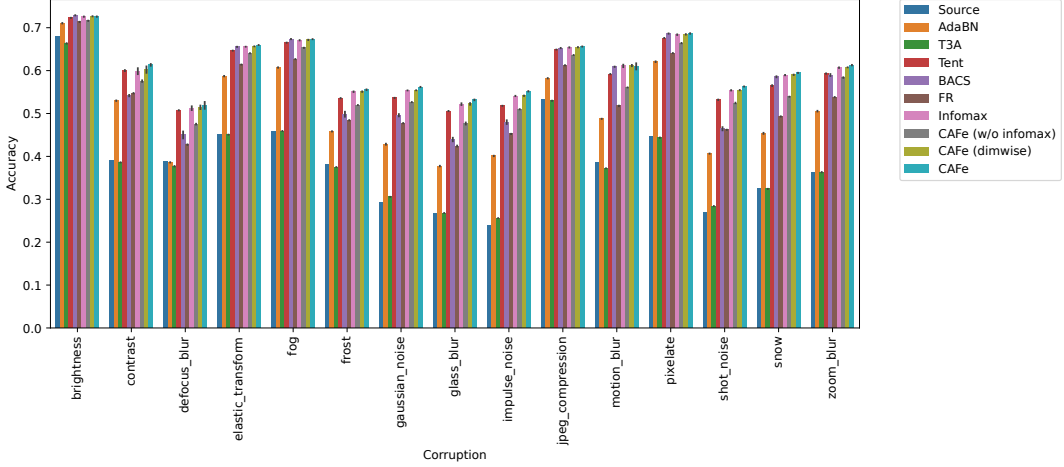


Figure 4: Test accuracy for each corruption type on the severity-wise sets of ImageNet-C. The accuracies are averaged over severity levels.

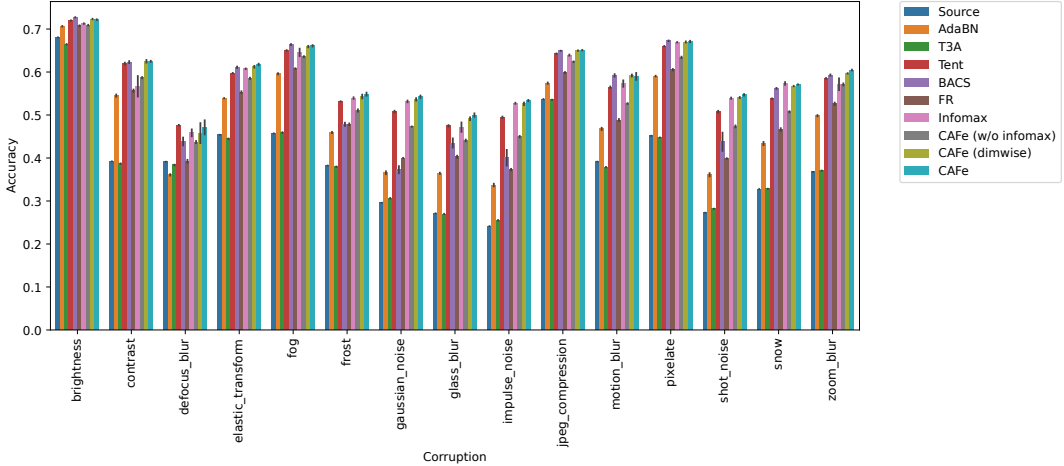


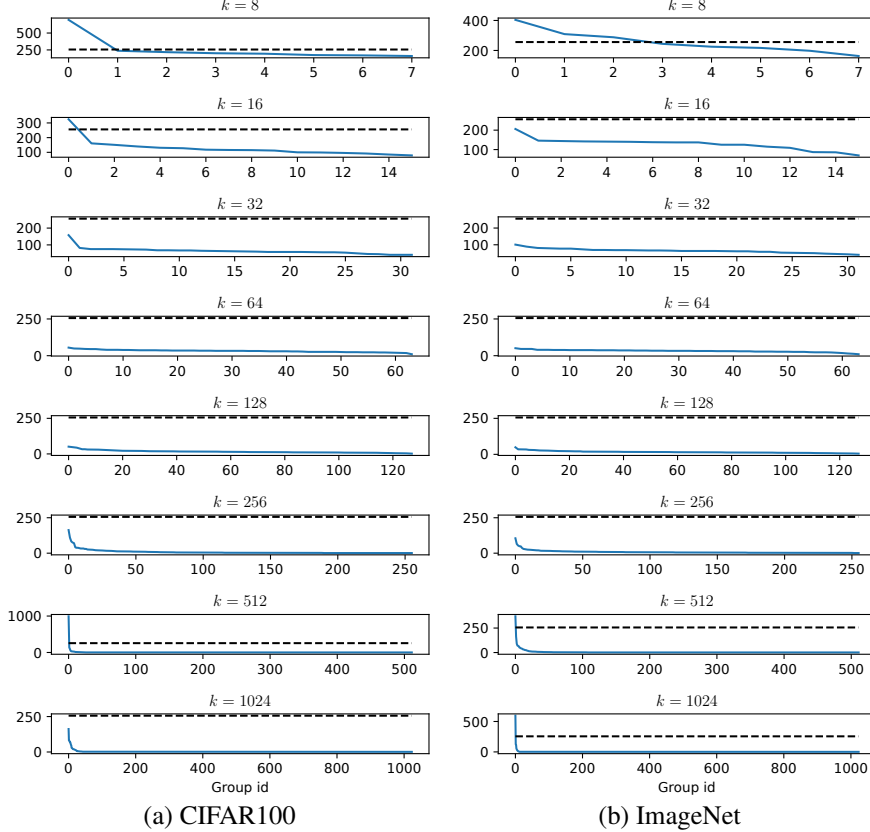
Figure 5: Test accuracy for each corruption type on the severity-mixed sets of ImageNet-C.

target covariance matrix Σ^t for the mini-batch degenerates and the feature alignment loss \mathcal{L}_a diverges. The corresponding entries in Tab. 4 are labeled N/A.

C.3 Mini-batched Online TTA

In the experiment described in Sec. 5.5 and Sec. 5.6, we ran TTA on the target dataset for one epoch and then evaluated it on the same target dataset, where each sample in the target dataset had to be accessed twice. However, there may be a situation in which we cannot access the whole target dataset at once. In this section, we describe performing TTA in a mini-batched online manner. Here, each target mini-batch can be accessed only one time. In other words, for each mini-batch, we perform one step of TTA optimization and then make a prediction on the mini-batch. This mini-batched online procedure is computationally efficient because we can discard the mini-batch after the prediction.

Tab. 5 and Tab. 6 show the test accuracy on CIFAR10/100-C and ImageNet-C/R evaluated in a mini-batched online manner. Compared with the offline TTA (Tab. 1 and Tab. 2), the accuracies deteriorated in most cases because the target mini-batches were predicted in the beginning with an insufficiently adapted model. However, CAFe had the best accuracy in most cases.



(a) CIFAR100

(b) ImageNet

Figure 6: Size of each group of feature dimensions for each k . The group ids are sorted in descending order of group size. The blue and dashed black lines indicate the group size and batch size ($= 256$).

Table 5: Test accuracy [%] on CIFAR10/100-C with mini-batched online TTA.

Method	CIFAR10-C		CIFAR100-C	
	Separated	Mixed	Separated	Mixed
Source	63.75	63.46 ± 0.61	34.24	34.16 ± 0.20
AdaBN [14]	80.04 ± 0.03	67.94 ± 0.16	50.72 ± 0.01	38.20 ± 0.09
T3A [19]	66.02 ± 0.02	63.92 ± 0.42	36.05 ± 0.07	34.10 ± 0.49
Tent [17]	79.31 ± 0.05	68.57 ± 0.25	50.04 ± 0.07	39.00 ± 0.09
BACS [18]	79.67 ± 0.05	68.28 ± 0.47	50.60 ± 0.07	38.98 ± 0.06
FR [27]	77.87 ± 0.11	68.65 ± 0.87	47.93 ± 0.05	38.70 ± 0.01
Infomax [30]	78.04 ± 0.10	68.80 ± 0.62	48.49 ± 0.05	38.62 ± 0.37
CAFe (w/o infomax)	77.90 ± 0.11	69.08 ± 0.34	48.13 ± 0.03	38.59 ± 0.37
CAFe (dimwise)	78.04 ± 0.10	68.91 ± 0.34	48.50 ± 0.06	38.86 ± 0.20
CAFe	78.18 ± 0.13	69.34 ± 0.43	48.64 ± 0.03	39.22 ± 0.28

C.4 SVHN and MNIST

We adapted the model pre-trained on SVHN [45] to MNIST [46], which are often used in domain adaptation studies. The details of these datasets are described in Appendix B. Tab. 7 shows that CAFe outperformed the other TTA methods and that CAFe (dimwise) performed the best.

C.5 Adapting to the Same Distribution

There may also be a situation in which the source and target distributions are the same, but we do not know in advance. Here, we performed TTA on a target domain identical to the source domain. We

Table 6: Test accuracy [%] on ImageNet-C/R with mini-batched online TTA.

Method	Separated	ImageNet-C		ImageNet-R
		Severity-mixed	All-mixed	
Source	39.14	39.43 ± 0.00	39.16 ± 0.01	36.17
AdaBN [14]	50.55 ± 0.01	48.02 ± 0.20	39.65 ± 0.10	40.02 ± 0.10
T3A [19]	39.05 ± 0.01	39.28 ± 0.03	37.46 ± 0.09	35.09 ± 0.12
Tent [17]	56.91 ± 0.02	54.66 ± 0.20	43.55 ± 0.30	42.23 ± 0.05
BACS [18]	57.25 ± 0.06	55.40 ± 0.27	37.71 ± 0.89	41.87 ± 0.34
FR [27]	51.22 ± 0.02	48.72 ± 0.20	40.11 ± 0.08	40.18 ± 0.03
Infomax [30]	58.22 ± 0.03	56.40 ± 0.19	45.80 ± 0.29	44.49 ± 0.06
CAFe (w/o infomax)	55.95 ± 0.04	53.13 ± 0.14	43.23 ± 0.20	39.90 ± 0.06
CAFe (dimwise)	58.21 ± 0.02	56.35 ± 0.20	45.61 ± 0.28	44.39 ± 0.05
CAFe	58.76 ± 0.04	56.90 ± 0.12	46.92 ± 0.34	43.76 ± 0.14

Table 7: Test accuracy on adapting SVHN to MNIST.

Method	Accuracy [%]
Source	73.15
AdaBN [14]	70.58 ± 0.61
T3A [19]	76.31 ± 0.10
Tent [17]	78.03 ± 0.36
BACS [18]	86.10 ± 0.29
FR [27]	83.61 ± 0.48
Infomax [30]	84.89 ± 0.05
CAFe (w/o infomax)	78.25 ± 0.24
CAFe (dimwise)	87.65 ± 0.35
CAFe	87.15 ± 0.21

adapted the source model pre-trained on CIFAR10/100 and ImageNet to their test split. Tab. 8 shows that CAFe does not largely deteriorate accuracy as the baselines.

C.6 Effect of the bias constant of CAFe

Let us examine the effect of the bias constant ϵ that is used for stability in Eq. (8). Tab. 9 shows the adapted accuracy on CIFAR10/100-C (Mixed) and ImageNet-C (All-mixed). For CIFAR10-C, the accuracies are N/A for $\epsilon \leq 10^{-6}$ due to degeneration. This is because CIFAR10 is relatively easier than the other datasets and the source model pre-trained on CIFAR10 uses only a small subspace of the feature space. On the other hand, for CIFAR100-C and ImageNet-C, the accuracies are not largely affected by ϵ even when $\epsilon = 0$. This is because the source statistics do not degenerate and the variances along the principal components do not need to be clipped using Eq. (8).

Table 8: Test accuracy [%] on the same distribution.

Method	CIFAR10	CIFAR100	ImageNet
Source	90.52	63.61	76.15
AdaBN [14]	89.08 ± 0.19	61.12 ± 0.32	75.64 ± 0.08
T3A [19]	90.43 ± 0.04	62.59 ± 0.12	71.70 ± 0.05
Tent [17]	89.41 ± 0.05	61.88 ± 0.11	75.97 ± 0.10
BACS [18]	89.58 ± 0.04	62.47 ± 0.13	76.38 ± 0.05
FR [27]	89.42 ± 0.07	61.59 ± 0.13	75.70 ± 0.03
Infomax [30]	89.55 ± 0.04	62.28 ± 0.07	76.02 ± 0.01
CAFe (w/o infomax)	89.43 ± 0.02	61.66 ± 0.08	75.50 ± 0.03
CAFe (dimwise)	89.56 ± 0.03	62.28 ± 0.06	76.04 ± 0.01
CAFe	89.59 ± 0.06	62.30 ± 0.13	75.97 ± 0.05

Table 9: Test accuracy [%] vs the bias constant ϵ . N/A means that the feature alignment loss \mathcal{L}_a diverged.

ϵ	CIFAR10-C (Mixed)	CIFAR100-C (Mixed)	ImageNet-C (All-mixed)
0	N/A	39.89 ± 0.72	48.57 ± 0.18
10^{-8}	N/A	39.83 ± 0.42	48.53 ± 0.30
10^{-7}	N/A	38.13 ± 2.73	48.63 ± 0.16
10^{-6}	N/A	39.77 ± 0.30	48.46 ± 0.08
10^{-5}	70.06 ± 0.25	40.01 ± 0.36	48.55 ± 0.26
10^{-4}	69.61 ± 0.72	40.27 ± 0.45	48.56 ± 0.26
10^{-3}	69.30 ± 0.17	39.83 ± 0.36	48.72 ± 0.08
10^{-2}	69.07 ± 0.34	39.13 ± 0.35	49.39 ± 0.28

Table 10: Test accuracy [%] on the target datasets adapted with DANN [8]. The accuracies of the source model and CAFE are also shown for comparison.

Method	CIFAR10-C (Mixed)	CIFAR100-C (Mixed)	ImageNet-C (All-mixed)	ImageNet-R
Source	63.46 ± 0.61	34.16 ± 0.20	39.16 ± 0.01	36.17
DANN	69.95 ± 0.61	38.63 ± 0.36	45.42 ± 0.63	40.02 ± 0.50
CAFE	70.06 ± 0.25	40.01 ± 0.36	48.55 ± 0.26	44.94 ± 0.19

C.7 Unsupervised domain adaptation

We additionally adapted classifiers to the target domains in the UDA setting, which allows access to the source and target datasets simultaneously. We used DANN [8], which is a representative UDA method. DANN employs a discriminator that takes the feature representations of the classifier and discriminates which domains they are from. By training the classifier and the discriminator adversarially, the classifier is expected to be able to learn domain-invariant feature representations. The discriminator we used is composed of three BN and fully-connected layers with ReLU activation whose numbers of the hidden dimensions are 1,024. We fine-tuned the source-pretrained classifiers with DANN. For the CIFAR experiments, we set `batch_size` = 128, `learning_rate` = 0.001 and `momentum` = 0.8. For the ImageNet experiments, we set `batch_size` = 64, `learning_rate` = 0.001 and `momentum` = 0.8. We trained DANN for 400 iterations for CIFAR10/100-C and 20,000 iterations for ImageNet-C/R. Tab. 10 reports the best accuracy. Compared with the TTA results in Tab. 1 and 2, it is clear that DANN improved the target accuracy more than the source model did. However, CAFE outperformed DANN. This is because the discriminator of DANN has to learn from scratch. The maximum number of iterations we trained for is one epoch based on the number of the source data. One epoch is insufficient for the discriminator to learn the domain discrimination. This suggests that DANN must be trained for a number of epochs for it to gain in accuracy.

D Algorithm of CAFE

Alg. 1 and Alg. 2 describe the procedure of CAFE.

Algorithm 1 Algorithm of CAFE (Pre-computing source statistics).

- # These steps are done in the source environment.
- Input:** Source-pretrained model $f_\theta = h_\psi \circ g_\phi$, source dataset $\{\mathbf{x}_i^s\}$
- Output:** Feature group G_1, \dots, G_k , source feature statistics for each group $\{\boldsymbol{\mu}_{G_i}^s\}_{i=1}^k, \{\boldsymbol{\Sigma}_{G_i}^s\}_{i=1}^k$
- Extract feature $\mathbf{z}_i^s = g_\phi(\mathbf{x}_i^s)$ for each sample.
- Compute the source feature statistics $\boldsymbol{\mu}^s$ and $\boldsymbol{\Sigma}^s$ with Eq. (2).
- Compute the adjacency matrix $A_{ij} = |\boldsymbol{\Sigma}_{ij}^s| / \sqrt{\boldsymbol{\Sigma}_{ii}^s \boldsymbol{\Sigma}_{jj}^s}$.
- Split the feature dimensions $\mathcal{V} = \{1, \dots, d\}$ into k groups G_1, \dots, G_k by spectral clustering according to the adjacency matrix A .
- Extract elements corresponding to each G_i from $\boldsymbol{\mu}^s$ and $\boldsymbol{\Sigma}^s$, denoted by $\boldsymbol{\mu}_{G_i}^s$ and $\boldsymbol{\Sigma}_{G_i}^s$.

Algorithm 2 Algorithm of CAFe (TTA step).

These steps are done in the target environment without access to the source dataset.

Input: Source-pretrained model $f_\theta = h_\psi \circ g_\phi$, unlabeled target dataset $\{\mathbf{x}_i^t\}$, feature group G_1, \dots, G_k , source feature statistics for each group $\{\boldsymbol{\mu}_{G_i}^s\}_{i=1}^k, \{\boldsymbol{\Sigma}_{G_i}^s\}_{i=1}^k$

Output: Target-adapted model $f_{\theta'}$

Compute the eigenvalues $\lambda_{G_i}^1, \dots, \lambda_{G_i}^{|G_i|}$ and eigenvectors V_{G_i} of the source covariance matrix $\boldsymbol{\Sigma}_{G_i}^s$ for each G_i .

Clip the eigenvalues with Eq. (8).

Compute the transformed source statistics $\tilde{\boldsymbol{\mu}}_{G_i}^s$ and $\tilde{\boldsymbol{\Sigma}}_{G_i}^s$ with Eq. (10).

for each mini-batch $\{\mathbf{x}_i^t\}_{i=1}^B$ **do**

 Extract feature $\mathbf{z}_i^t = g_\phi(\mathbf{x}_i^t)$ and make prediction $\hat{p}_i = \text{softmax}(h_\psi(\mathbf{z}_i^t))$ for each sample.

 Compute the batch statistics $\boldsymbol{\mu}^t$ and $\boldsymbol{\Sigma}^t$ analogously to Eq. (2).

 Extract elements from $\boldsymbol{\mu}^t$ and $\boldsymbol{\Sigma}^t$ corresponding to each G_i , denoted by $\boldsymbol{\mu}_{G_i}^t$ and $\boldsymbol{\Sigma}_{G_i}^t$.

 Compute the transformed target statistics $\tilde{\boldsymbol{\mu}}_{G_i}^t$ and $\tilde{\boldsymbol{\Sigma}}_{G_i}^t$ with Eq. (9).

 Compute the feature alignment loss \mathcal{L}_a with the transformed statistics $\tilde{\boldsymbol{\mu}}_{G_i}^t, \tilde{\boldsymbol{\Sigma}}_{G_i}^t, \tilde{\boldsymbol{\mu}}_{G_i}^s, \tilde{\boldsymbol{\Sigma}}_{G_i}^s$ by Eq. (7).

 Compute the infomax loss \mathcal{L}_{IM} with Eq. (5).

 Update the feature extractor g_ϕ to minimize $\mathcal{L}_a + \mathcal{L}_{IM}$.

end for
